

# REV-ERB $\alpha$ ameliorates heart failure through transcription repression

Lilei Zhang,<sup>1,2</sup> Rongli Zhang,<sup>2</sup> Chih-Liang Tien,<sup>1</sup> Ricky E. Chan,<sup>3</sup> Keiki Sugi,<sup>2</sup> Chen Fu,<sup>4</sup> Austin C. Griffin,<sup>2</sup> Yuyan Shen,<sup>2</sup> Thomas P. Burris,<sup>5</sup> Xudong Liao,<sup>2</sup> and Mukesh K. Jain<sup>2</sup>

<sup>1</sup>Department of Molecular and Human Genetics, Baylor College of Medicine, Houston, Texas, USA. <sup>2</sup>Case Cardiovascular Research Institute, Department of Medicine, Harrington Heart and Vascular Institute, <sup>3</sup>Institute for Computational Biology, and <sup>4</sup>Department of Genetics and Genome Sciences, Case Western Reserve University, Cleveland, Ohio, USA. <sup>5</sup>Department of Pharmacology and Physiology, Saint Louis University, St. Louis, Missouri, USA.

**A cure for heart failure remains a major unmet clinical need, and current therapies targeting neurohormonal and hemodynamic regulation have limited efficacy. The pathological remodeling of the myocardium has been associated with a stereotypical gene expression program, which had long been viewed as the consequence and not the driver of the disease until very recently. Despite the advance, there is no therapy available to reverse the already committed gene program. Here, we demonstrate that transcriptional repressor REV-ERB binds near driver transcription factors across the genome. Pharmacological activation of REV-ERB selectively suppresses aberrant pathologic gene expression and prevents cardiomyocyte hypertrophy. In vivo, REV-ERB $\alpha$  activation prevents development of cardiac hypertrophy, reduces fibrosis, and halts progression of advanced heart failure in mouse models. Thus, to our knowledge, modulation of gene networks by targeting REV-ERB $\alpha$  represents a novel approach to heart failure therapy.**

## Introduction

Heart failure (HF) affects more than 5 million people in the US, and the incidence is still rising (1). It is associated with a ~50% mortality within 5 years of diagnosis despite advances in medical care (2). Current state-of-the-art therapy aims to reduce the neurohormonal stress and improves hemodynamics. It has long been known that the remodeling of the heart is associated with a stereotypical exchange of gene expression programs driven by key transcription factors (TFs) (3). However, how to selectively suppress the aberrant gene program coordinated by multiple TFs in a global fashion is not known, and thus, an effective strategy to counteract HF is unavailable; therapies directly targeting transcriptional control of the aberrant gene program are lacking.

REV-ERB $\alpha$  is a transcriptional repressor with diverse roles in different tissues (4). Recent studies in the fibroblasts and liver suggested that REV-ERB $\alpha$  preferentially binds to open chromatin structure and it may tether to tissue specific factors independent of its own DNA binding domain (5, 6). These features suggest that REV-ERB $\alpha$  may be a unique “brake” of aberrantly activated gene programs in the disease state through multiple TFs in a tissue-specific manner. However, REV-ERB $\alpha$ 's role in the heart remains poorly understood, with one recent report indicating that synthetic agonists can attenuate cardiac hypertrophy (7). The role of REV-ERB $\alpha$  in clinically relevant models of HF and the molecular basis for its actions remain unknown.

## Results

To start deciphering its function in the heart, we analyzed our previously reported REV-ERB $\alpha$  cistrome in the heart (8). Similar to previous reports in the liver and macrophages, the top enriched motifs are REV-ERB $\alpha$ 's own DNA cognate sites (ROR and Revrb, DR2), followed by tissue-specific factor sites, MEF2a and MEF2c (Figure 1) (6, 9). MEF2a and MEF2c are known drivers of the cardiac hypertrophy gene program, and previous studies show that ectopic expression of MEF2a or MEF2c in the heart leads to dilated cardiomyopathy and HF (10, 11). They are also the top enriched enhancer motifs that undergo chromatin state switching in a murine cardiac pressure overload model (12). The colocalization of REV-ERB $\alpha$  to MEF2a and MEF2c suggests that it may specifically repress the aberrantly activated gene program during cardiac hypertrophy and HF driven by MEF2a and MEF2c.

**Conflict of interest:** The authors have declared that no conflict of interest exists.





**Submitted:** May 16, 2017

**Accepted:** August 3, 2017

**Published:** September 7, 2017

**Reference information:**

*JCI Insight.* 2017;2(17):e95177. <https://doi.org/10.1172/jci.insight.95177>.

Motif	Name	P - Value	%
	ROR	1e-307	11.30
	Reverb, DR2	1e-201	9.56
	Mef2a	1e-38	6.57
	Mef2c	1e-36	6.35

**Figure 1. Top enriched motifs of REV-ERB $\alpha$  cistrome in the heart.** The percent of target sequences with motif is shown in the % column.

SR9009 is a validated synthetic REV-ERB agonist, which facilitates REV-ERB $\alpha$  to recruit its corepressor NCoR and repress downstream targets (13). We first tested the effect of SR9009 directly in primary cardiomyocytes in vitro. In neonatal rat ventricular myocytes (NRVMs), SR9009 effectively blocked the phenylephrine-induced (PE-induced) cellular hypertrophy and expression of cellular stress markers (Figure 2, A–C). Further, another independently developed, structurally distinct REV-ERB agonist, GSK4112, also showed a similar result (Figure 2D). Thus, activation of REV-ERB leads to blockade of cardiomyocyte hypertrophy and cellular stress in a cell-autonomous fashion. We subsequently focused our study using SR9009 due to its higher efficacy and favorable in vivo pharmacodynamics (13).

To elucidate the molecular mechanisms underlying REV-ERB $\alpha$  effects, we performed RNA-Seq on NRVM at baseline and after PE stimulation (4 hours [hr] and 48 hr) in the presence or absence of SR9009 (SR or Veh were given 24 hr prior to PE). All original RNA-Seq data were deposited in the NCBI's Gene Expression Omnibus (GEO GSE98575). All the genes with pairwise differential expression between SR9009 and vehicle-treated (Veh-treated) groups at each time point were analyzed using Gene Set Enrichment Analysis (GSEA), and the genes in the altered pathways (defined by family-wise error rate [FWER] < 0.25) were further analyzed using unsupervised hierarchical clustering (Figure 3A). Veh-PE-treated groups showed a shift in gene expression patterns at 4 hr that continued to deviate from the baseline with time. In contrast, the SR-treated groups displayed an expression pattern more similar to the baseline groups, despite the persistent exposure to PE for 48 hr. We then compared the number of differentially expressed genes in each group (vs. Veh-baseline and defined by changes > 1.5-fold and  $q < 0.005$ ). We found that, while the Veh-treated groups have about equal number of genes being up- or downregulated, the SR-treated groups have twice as many genes being downregulated than upregulated, consistent with its role as a transcriptional repressor. Further, as the total number of differential genes continue to increase from 4 hours of vehicle treatment (Veh-4h) to Veh-48h, indicative of the continuation of the hypertrophy process, the SR-48h had significantly fewer differentially expressed genes compared with the early time point SR-4h, suggesting the hypertrophy process was blocked at the transcriptional level (Figure 3B). Representative genes with REV-ERB $\alpha$  and MEF2a cooccupancy and transcription repression by SR9009 treatment were shown (Figure 3, C and D).

Using GSEA, we analyzed the differentially expressed genes between SR9009 and Veh at each time point (Figure 4A and Supplemental Table 1; supplemental material available online with this article; <https://doi.org/10.1172/jci.insight.95177DS1>). Baseline and 4-hr time points were combined, as they showed the same top enriched pathway (hypertrophic cardiomyopathy) when analyzed individually (the individually analyzed result is available in Supplemental Table 1). Veh-treated cells showed an enrichment for cardiomyopathy and contractile pathways at baseline and 4 hr. The activation of hypertrophic pathways at baseline in the Veh-treated group suggests that, under the current culture condition (without PE), there is a low level of spontaneous hypertrophy that is prevented by SR9009 treatment. Forty-eight hr after PE exposure, the Veh-treated group showed an enrichment for remodeling and inflammation pathways most consistent with the advanced hypertrophic stage, while the SR9009-treated group showed an enrichment of cellular metabolism pathways known to be downregulated in the failing heart. These results suggest that the REV-ERB agonist exerts its effect mainly through gene repression and that the difference between the SR9009 and Veh groups lies in the genes and pathways that are up- or downregulated in the Veh groups and less changed in the SR9009 groups, as *Nppa* and *Nppb* show in Figure 2D.

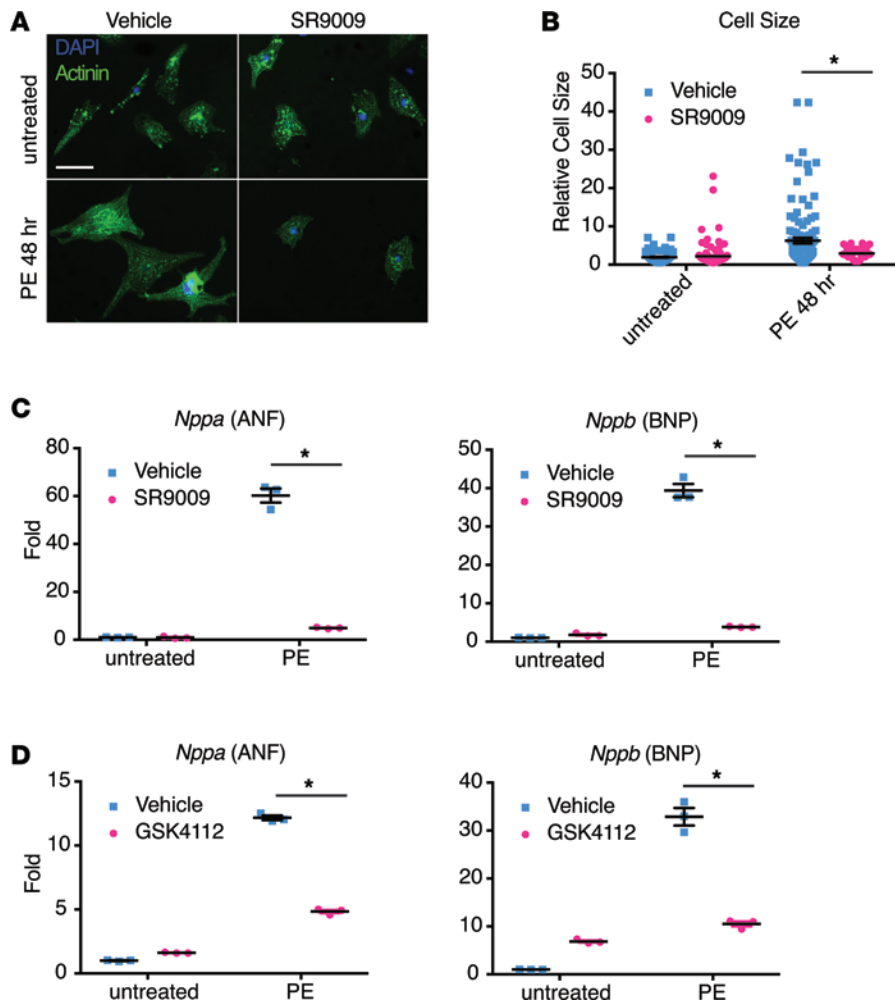


**Figure 2. REV-ERB agonist prevented the phenylephrine-induced (PE-induced) cardiomyocyte hypertrophy through transcriptional repression of the fetal gene program.** (A–C) Neonatal rat ventricular myocytes (NRVMs) were pretreated with vehicle or SR9009 for 24 hours and then treated with PE for 48 hours. (A) Immunofluorescent staining with  $\alpha$ -actinin (green). Scale bar: 30  $\mu$ M. (B) Quantification of cell size.  $*P = 0.02$ ,  $n = 42$ –114. (C) qPCR of *Nppa* and *Nppb*.  $*P = 0.00009$  (*Nppa*),  $*P = 0.00007$  (*Nppb*),  $n = 3$ . (D) NRVMs were pretreated with vehicle or GSK4112 for 24 hours and then treated with PE for 48 hours. qPCR of *Nppa* and *Nppb*.  $*P = 0.00001$  (*Nppa*),  $*P = 0.0003$  (*Nppb*),  $n = 3$ . Statistical differences were determined by 2-tailed Student's *t* test. Data are presented as mean  $\pm$  SEM. Multiple comparison is corrected for by using Holm-Sidak method, with  $\alpha = 0.05$ .

As a large number of genes involved in the fatty acid oxidation pathway maintained their expression with SR9009 treatment (Figure 4B), we investigated the role of PDK4, an important modulator of the pathway (14). Interestingly, we observed a cooccupation of MEF2A and REV-ERB $\alpha$  on the promoter and an enhancer element at the *Pdk4* locus (Figure 4C). In addition, PE represses the expression of *Pdk4*, which is ameliorated by SR9009 treatment, as seen in our RNA-Seq result (Figure 4D). PDK4 is likely one of the main targets of REV-ERB $\alpha$  during cardiac metabolic remodeling.

Given the strong effect of SR9009 in blocking the cellular remodeling in response to neurohormonal stress, we next tested the role of REV-ERB $\alpha$  activation in vivo using the classical pressure overload model. We started daily i.p. injection of SR9009 or Veh 1 day after transaortic constriction (TAC, 27 gauge) surgery and monitored cardiac hypertrophy and function by echocardiogram for 6 weeks. The SR9009 dose (10 mg/kg/day) was previously established and displayed no apparent toxicity (15). We found that, while mice treated with Veh demonstrated a gradual reduction in cardiac function (ejection fraction [EF] = 52.8% at 4 weeks and EF = 46.9% at 6 weeks), SR9009-treated animals maintained normal cardiac function (EF = 61.4% at 4 weeks and EF = 60.6% at 6 weeks,  $P = 0.03$ ) (Figure 5, A–D).

The SR9009-treated group also showed significantly less cardiac hypertrophy measured by echocardiogram. The corrected left ventricle mass (LVm) showed a continued increase in the Veh-treated group (LVm = 129.6 mg at 4 weeks and LVm = 139.2 mg at 6 weeks), which is attenuated in the SR9009-treated group (LVm = 111.4 mg at 4 weeks [ $P = 0.01$ ] and LVm = 114.8 mg at 6 weeks [ $P = 0.02$ ]). The left ventricle posterior wall thickness (LVPW; diastole [d]) and intraventricular septum thickness (IVS; d) showed similar trends (Figure 6A). These findings were later confirmed by autopsy performed 6 weeks after TAC by heart weight and muscle fiber size analyses using wheat germ agglutinin staining on cryopreserved sections (Figure 6, B–E). Furthermore, we observed drastically reduced intracardiac fibrosis

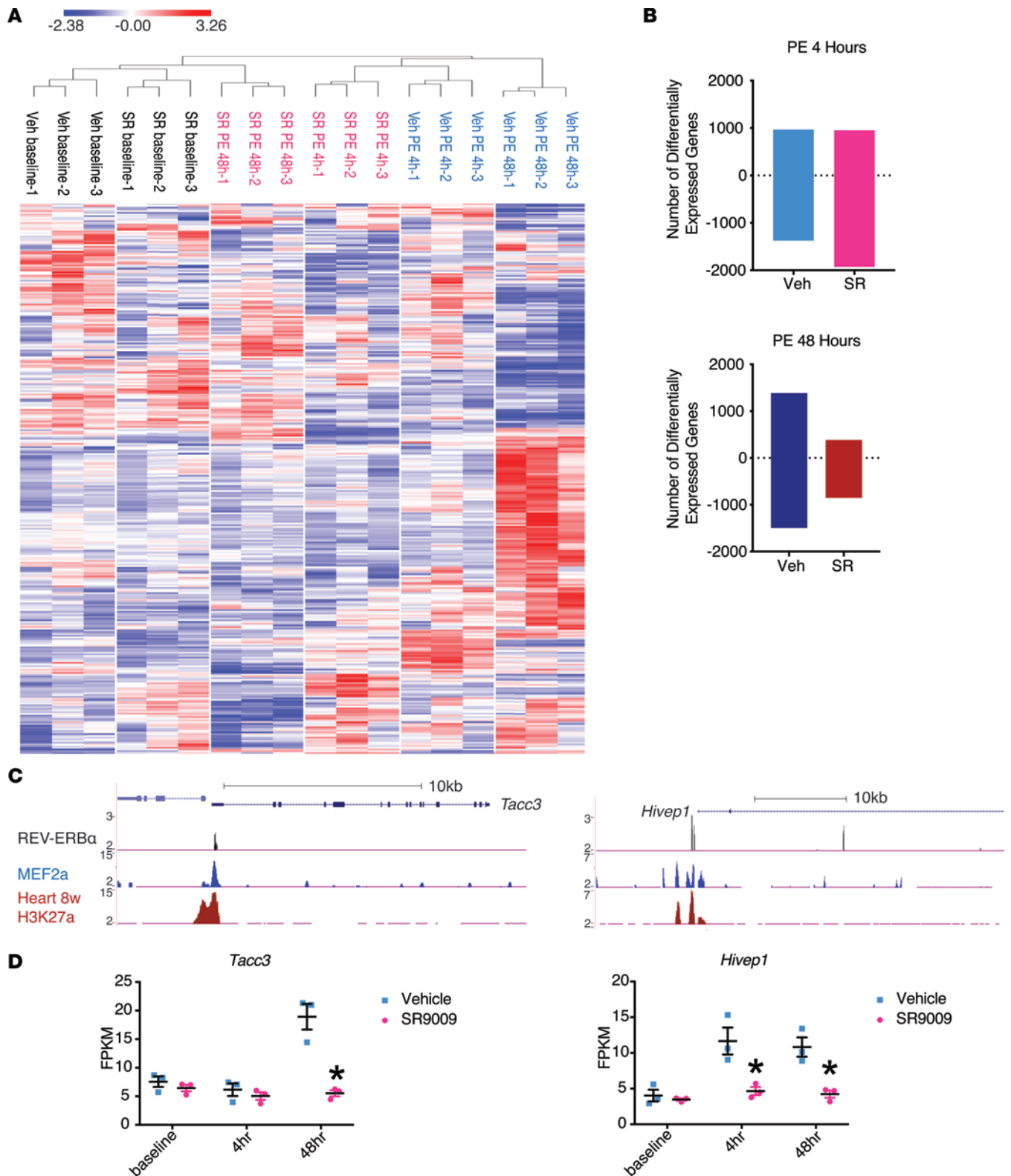


**Figure 3. REV-ERB $\alpha$  regulates gene program during cardiomyocyte hypertrophy in vitro via transcription repression.** (A and B) RNA-Seq analysis. Neonatal rat ventricular myocytes (NRVMs) were pretreated with vehicle (Veh) or SR9009 (SR) for 24 hours and then treated with phenylephrine (PE) for 48 hours. Samples were collected at 0, 4, and 48 hours after PE treatment.  $n = 3$ . (A) Heat map with unsupervised hierarchical clustering. Three hundred and twenty-four genes from all the pathways showing a pairwise differential expression, defined by FWER,  $P < 0.250$ . (B) The number of differentially expressed genes comparing to vehicle baseline. The number of upregulated genes are shown as positive, and the number of downregulated genes are shown as negative. (C) ChIP-Seq gene tracks from REV-ERB $\alpha$  (black), MEF2a (blue), and H3K27a (red). MEF2a data is a previously published result from HL-1 cells. H3K27a is part of the ENCODE data from adult mice hearts (28, 29). (D) Fragments per kilobase of transcript per million mapped reads (FPKM). \* $P = 0.013$  (*Tacc3*), \* $P = 0.047$  (*Hivp1* 4 hr), \* $P = 0.031$  (*Hivp1* 48 hr),  $n = 3$ . Statistical differences were determined by 2-tailed Student's  $t$  test. Data are presented as mean  $\pm$  SEM. Multiple comparison is corrected for by using Holm-Sidak method, with  $\alpha = 0.05$ .

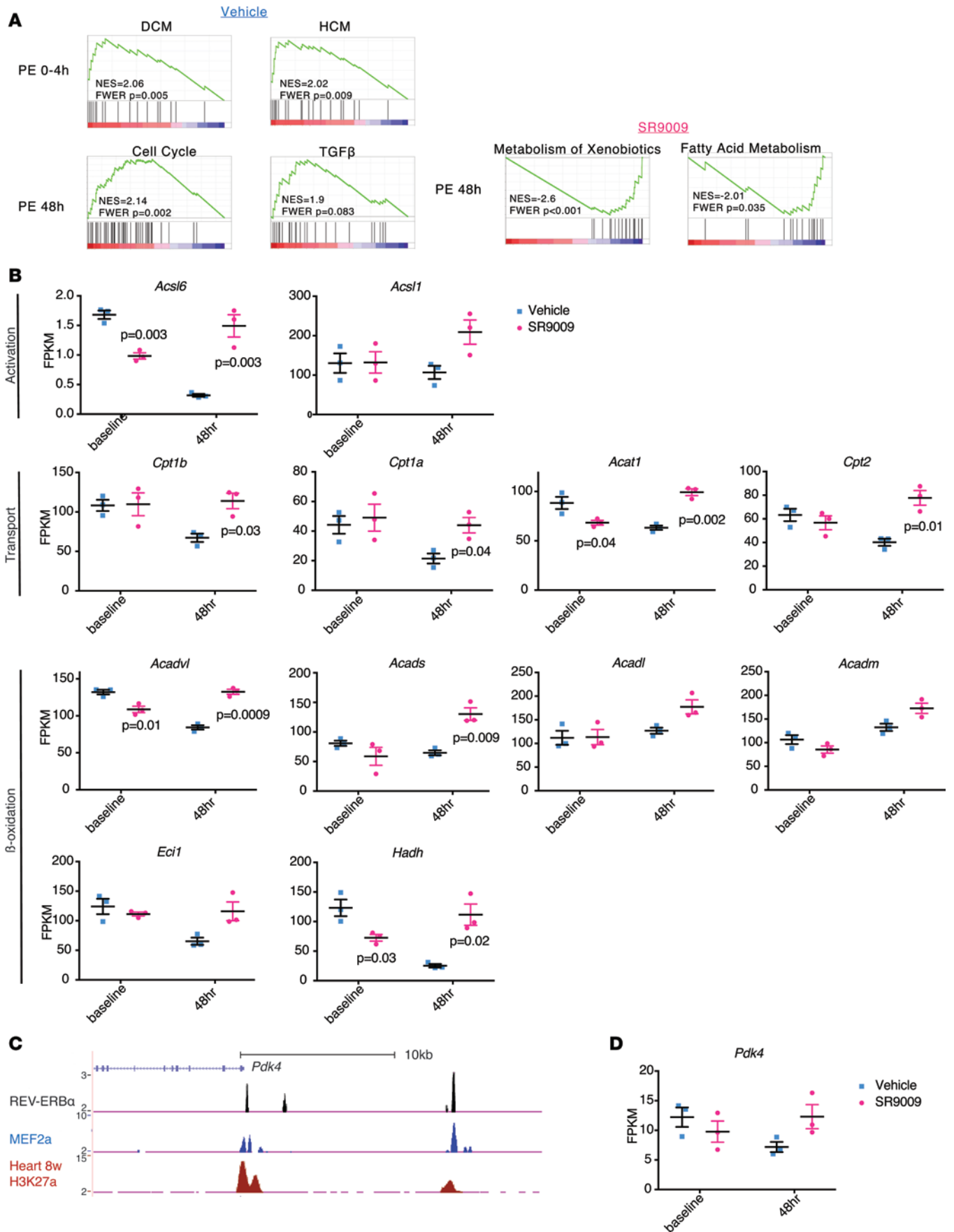




**Figure 4. REV-ERB $\alpha$  regulates major gene pathways during cardiomyocyte hypertrophy in vitro.** RNA-Seq analysis. **(A)** Gene Set Enrichment Analysis (GSEA). The top pathways were shown and the complete list is in Supplemental Table 1. DCM, dilated cardiomyopathy; HCM, hypertrophic cardiomyopathy; NES, normalized enrichment score; FWER, family-wise error rate. **(B)** Fragments per kilobase of transcript per million mapped reads (FPKM),  $n = 3$ . Significant  $P$  values after correction for multiple comparison are indicated in the graph. Statistical differences were determined by 2-tailed Student's  $t$  test. Data are presented as mean  $\pm$  SEM. Multiple comparison is corrected for by using Holm-Sidak method, with  $\alpha = 0.05$ . **(C)** ChIP-Seq gene tracks from REV-ERB $\alpha$  (black), MEF2a (blue), and H3K27a (red). MEF2 data is a previously published result from HL-1 cells. H3K27a is part of the ENCODE data from adult mice hearts (28, 29). **(D)** FPKM of Veh- and SR9009-treated hearts at baseline and 48 hours after treatment.

in the SR9009-treated group. At the end of 6 weeks after TAC, the Veh-treated group showed an intramuscular fibrosis area of 10.3%, while the SR9009-treated groups showed no significant fibrosis, with an intramuscular fibrosis area of 1.1%,  $P = 0.003$  (Figure 6, F and G). Cell death quantified by TUNEL assay also indicated that there is more cell death in the Veh-treated group (27.8 tunnel positive cells per cross-section of the whole heart) than the SR9009-treated group (13.4 positives per cross-section of the whole heart,  $P = 0.002$ ) (Figure 6, H and I).

SR9009 is a drug given systemically and may potentially affect other systems, such as the vascular tone, although pressure overload itself is considered a relatively specific stress directly on the heart. To exclude the possibility that the improved cardiac function and reduced hypertrophy in vivo is associated with improvement in hemodynamics, we measured blood pressure using tail cuff and found there is no difference in mice receiving 4 weeks of Veh (mean arterial pressure [MAP] = 106 mmHg) or SR9009 (MAP = 115 mmHg,  $P = 0.24$ , Supplemental Figure 1A). Since there is a substantially improved fibrosis in the SR9009-treated heart, we also investigated if the in vivo protection is directly on cardiomyocytes or through cardiac fibroblasts (CFs). We found there is no difference in the TGF $\beta$ 1-induced inflammatory response of cultured CFs pretreated with Veh or SR9009 (Supplemental Figure 1, B and C). Further, we see no difference in capillary density after 6 weeks of TAC between Veh- and SR9009-treated groups, suggesting there is no secondary benefits through improved angiogenesis and microcirculation (Supplemental Figure 1D). Thus, REV-ERB agonism has a direct protection on the cardiomyocytes, consistent with our NRVM results in culture.

Using RNA-Seq, we found that in NRVM SR9009-treated cells showed an enrichment in metabolic pathways that are known to be downregulated in HF, in particular fatty acid metabolism, which accounts for 70% of the energy source in the normal heart. Also, SR9009 has previously been reported to increase mitochondrial number, function, and mitophagy in skeletal muscle (15). We then investigated if there is a direct induction of mitochondria metabolism by SR9009. However, even after 10 weeks after TAC in the mouse hearts, there is no difference in mitochondria number estimated by mtDNA to nuclear DNA ratio, no difference in morphology by electron microscopy, and no difference in oxidative phosphorylation (OXPHOS) measured by oxygen consumption rate (Supplemental Figure 1, E–G). These observations indicate that an improved energy metabolism is not the direct cause of REV-ERB-induced cardiac protection; rather, they support our cistrome and transcriptomic data that a pathological gene program is repressed in the cardiomyocytes.

We next sought to determine if REV-ERB $\alpha$  activation impacts the failing heart. Most interventions using animal models have focused on the outcome of disease prevention. However, patients often present with existing and sometimes late-stage HF; a potential therapy in human patients requires efficacy in treating established or even late-stage disease. To establish an HF model, we performed a 28-gauge TAC (more severe than the commonly used 27-gauge model) on a cohort of 18 mice (Figure 7). At 2 weeks after TAC, we observed an average EF of  $44\% \pm 1.3\%$  in all the surviving mice ( $n = 10$ ). We randomized them into 2 groups based on EF and treated 1 group with Veh (Group I) and another with SR9009 (Group II). At 6 weeks after TAC, Group II maintained cardiac function, with an EF of  $43.9\% \pm 5\%$ , while Group I dropped to  $29.1\% \pm 1.8\%$  ( $P = 0.01$ ). We then performed a cross-over, in which Group I received SR9009 and Group II received Veh, and we observed animals for an additional 5 weeks. Group I maintained an EF of  $29.8\% \pm 3.7\%$ , while Group II dropped to  $17.5\% \pm 2.3\%$  ( $P = 0.01$ ) (Figure 6, F and G). This result suggests that the REV-ERB $\alpha$  pathway can halt moderate and even severe HF.

Finally, we investigated if a similar modulatory role of REV-ERB $\alpha$  exists in human cardiomyocytes. We induced cellular hypertrophic response in human induced pluripotent stem cell-differentiated cardiomyocytes with endothelin-1 (ET-1) and monitored *NPPB* (BNP) expression with SR9009 or Veh pretreatment. Not too surprisingly, we observed a protective effect of SR9009, just as in the rodent cardiomyocytes (Figure 8).

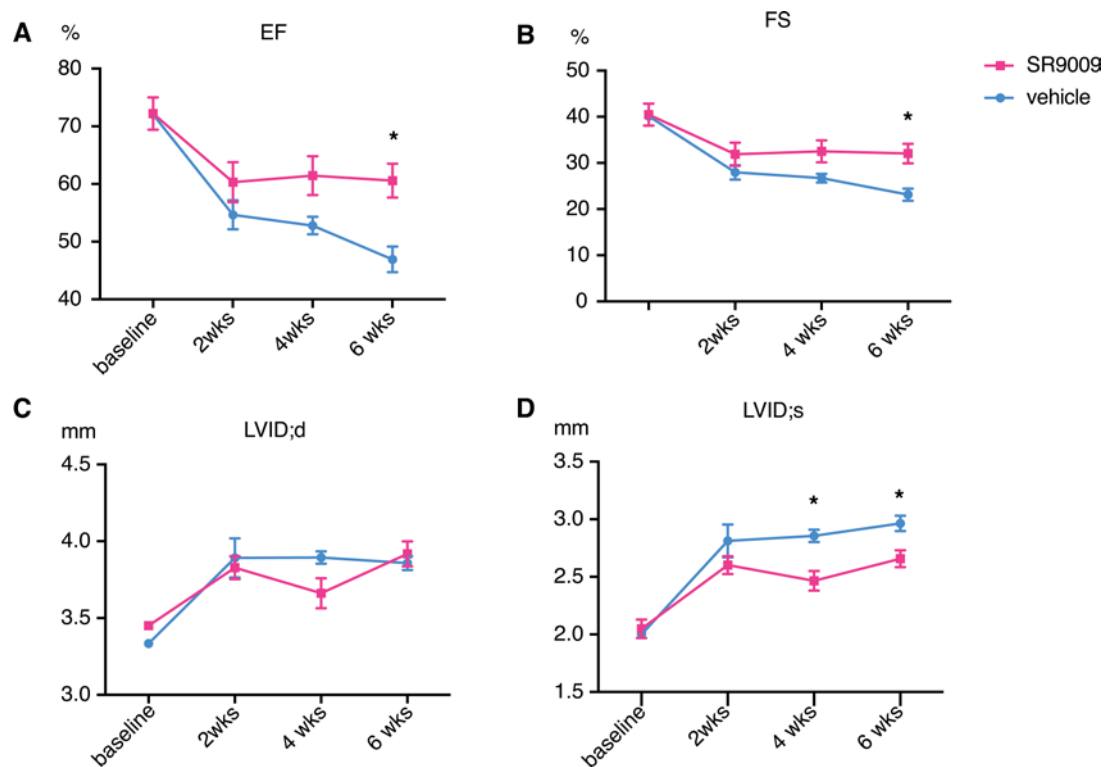


**Figure 5. REV-ERB agonist ameliorate cardiac dysfunction in pressure-overload models.** (A–D) Six-week followup of 27-gauge TAC performed on 8-week-old mice, vehicle, or SR9009, which were given daily starting 1 day after surgery.  $n = 5$ . (A) Ejection fraction (EF),  $*P < 0.05$ . (B) Fraction shortening (FS),  $*P < 0.05$ . (C) Left ventricle internal diameter end diastole. (D) Left ventricle internal diameter end systole.  $*P < 0.05$ . Statistical differences were determined by 2-tailed Student's  $t$  test. Data are presented as mean  $\pm$  SEM. Multiple comparison is corrected for by using Holm-Sidak method, with  $\alpha = 0.05$ .

## Discussion

Our study reveals that REV-ERB $\alpha$  is a key regulator of cardiac pathological remodeling and ameliorates HF, both in a preventative and therapeutic fashion, in rodent models. Mechanistically, we demonstrated that REV-ERB $\alpha$  colocalizes with driver TFs, such as MEF2a and MEF2c, and represses aberrant gene expression during cardiac pathological stress.

Multiple TFs and chromatin remodeling factors have been shown to participate in the cardiac hypertrophy gene program. Although it is still a topic of active debate, more recent evidence suggests that the activation of hypertrophic genes plays an adverse role in cardiac remodeling and is causal for the pathogenesis of HF (16). Despite the improved understanding, direct gene regulation has not been translated into efficacious therapy for HF, at least partly due to the lack of tools to coordinately manipulate multiple TFs in a spatial- and temporal-specific manner. Using heart tissue ChIP-Seq, we have found that REV-ERB $\alpha$  can colocalize with driver TFs and coordinate transcription repression at thousands of loci in the genome mediated by multiple TFs, which can prevent pathogenic switch of gene program. We realize that it is very possible that REV-ERB $\alpha$  has additional partners beyond MEF2a and MEF2c in the heart. A detailed study of the REV-ERB $\alpha$  cistrome in the purified cardiomyocytes is required to gain additional insight of its complete set of partners and targets during pathological remodeling of the heart. The mechanisms that allow REV-ERB $\alpha$  to colocalize with tissue-specific TFs and modulate the selective gene program during the disease process also warrant further investigation.

Several compounds have been generated to manipulate REV-ERB function (17). We chose to use SR9009 for its high efficacy and feasibility for in vivo studies. The specificity of SR9009 to REV-ERB has been shown to bind all 48 human nuclear receptors (13). Previously, SR9009 has been used in other studies and has demonstrated effects in shortening sleep, reducing anxiety, increasing skeletal muscle performance and endurance exercise, increasing oxygen consumption, and protecting against obesity induced by high fat diet (13, 15, 18). Due to its effect on mitochondria number, function, and mitophagy in skeletal muscle, as well as our GSEA results indicating an enriched expression in fatty acid metabolism, we tested the possibility of

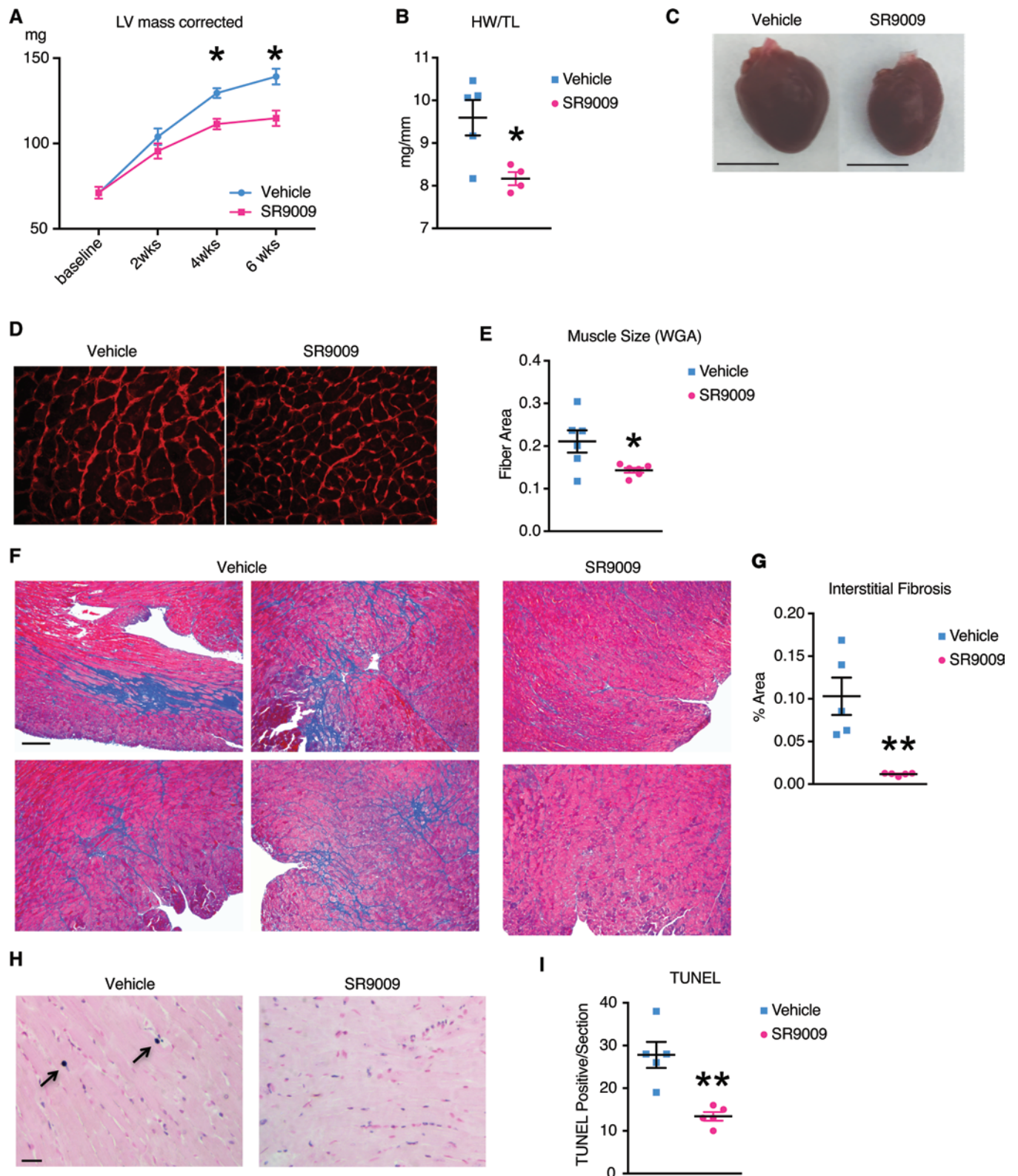
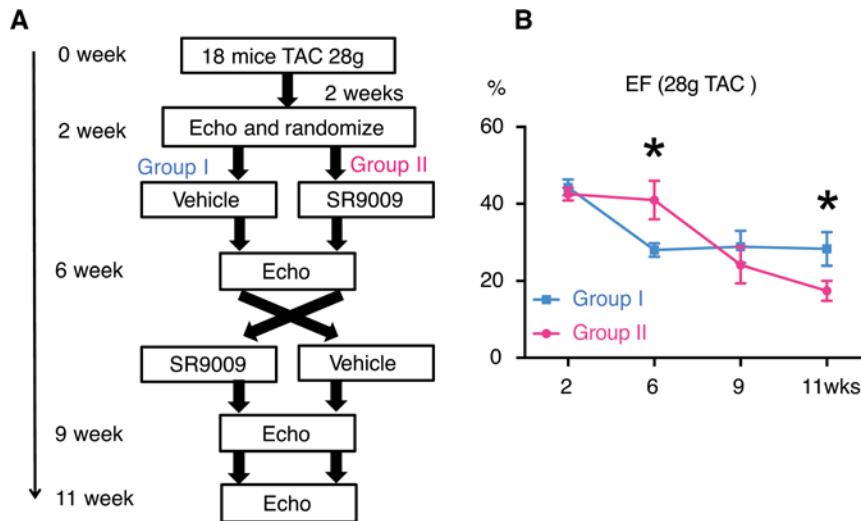


**Figure 6. REV-ERB agonist ameliorate cardiac hypertrophy in pressure overload models.** Six-week followup of 27-gauge TAC was performed on 8-week-old mice, vehicle, or SR9009, which were given daily starting one day after surgery.  $n = 5$ . **(A)** Left ventricle mass, corrected,  $*P < 0.05$ . **(B)** Heart weight normalized to tibia length,  $*P < 0.05$ . **(C)** Representative pictures of vehicle- and SR9009-treated hearts harvested at 6 weeks. Scale bar: 5 mm. **(D)** Wheat germ agglutinin staining. Scale bar: 30  $\mu\text{m}$ . **(E)** Quantified muscle fiber size in arbitrary units,  $*P < 0.05$ . **(F)** Fibrosis stained with Gomori Trichrome stain, representative pictures. Vehicle, left column and middle column. SR9009, right column. Scale bar: 400  $\mu\text{m}$ . **(G)** Quantification of fibrotic area. **(H)** TUNEL staining, representative picture. Scale bar: 20  $\mu\text{m}$ . **(I)** Quantification of TUNEL signal per section. Statistical differences were determined by 2-tailed Student's  $t$  test. Data are presented as mean  $\pm$  SEM. Multiple comparison is corrected for by using Holm-Sidak method, with  $\alpha = 0.05$ .





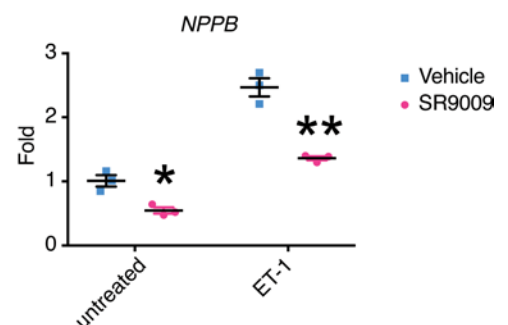
mitochondrial-driven cardiac protection. Our results indicate that there is no significant benefit directly associated with increased mitochondrial number or function. This difference may be due to tissue specificity or the particular type of injury being used. A more direct injury on the mitochondria, such as ischemia reperfusion, may induce more observable changes in the mitochondria.

REV-ERB is generally thought to be a repressor due to the lack of an activation domain, and we do see, globally, a more prominent effect in downregulation rather than upregulation of gene expression. It is likely that most upregulated genes are upregulated through an indirect mechanism. However, REV-ERB $\alpha$  has been demonstrated to be able to activate gene expression in vitro in an early study, and in the case of PDK4 and possibly other examples, an activator's role may be plausible (19). The detailed mechanism requires further investigation. In addition, PDK4 may be subjected to regulation at multiple posttranscriptional levels during cardiac hypertrophy, which is not directly associated with gene expression. However, it is likely that PDK4 plays a crucial role in coordinating a large number of genes involved in cardiac fatty acid metabolism, as previously reported, and dysregulation of PDK4 likely contributes to the metabolic remodeling during cardiac hypertrophy, which can be ameliorated by REV-ERB $\alpha$  agonism.

Although pressure overload is a relatively heart-specific injury model, other systems and cell types may play a significant role in the outcome. We show that there is no difference in blood pressure, mitochondria number/morphology/oxidation and phosphorylation, capillary density, or CFs, suggesting that the SR9009-treated hearts had preserved cardiac function due to less cardiomyocyte injury instead of any secondary benefit from improved hemodynamics, metabolism, microcirculation, or less-reactive CFs. Together with our result in NRVM, we conclude that REV-ERB activation has a direct protective effect in cardiomyocytes in a cell-autonomous fashion. We realize that fibrosis in vivo requires interaction between the cardiomyocytes and CFs, as well as other secretory factors. A more detailed study on the direct effect of SR9009 on cardiac fibrosis in vivo is warranted.

Mechanistically, REV-ERB activation is distinct from current neurohormonal modulation therapies and likely will provide nonoverlapping benefits to HF patients. We have shown that, in mice, the therapy

**Figure 8. REV-ERB agonist prevented the endothelin-1-induced (ET-1-induced) hypertrophy in human induced pluripotent stem cell-differentiated cardiomyocytes (iPS-CM).** iPS-CM were pretreated with vehicle or SR9009 for 24 hours and then treated with ET-1 for 48 hours. qPCR of *Nppb*. \* $P = 0.01$  (untreated), \*\* $P = 0.003$  (ET-1),  $n = 3$ . Statistical differences were determined by 2-tailed Student's  $t$  test. Data are presented as mean  $\pm$  SEM. Multiple comparison is corrected for by using Holm-Sidak method, with  $\alpha = 0.05$ .



is effective even in advanced disease — at least to prevent disease progression — despite of the persisting insult. Its efficacy in advanced disease is particularly attractive to provide medical management to end-stage HF patients in order to avoid or delay heart transplant or mechanical assisting device.

Finally, our nascent observation that the same protection of REV-ERB agonist exists in the human cardiomyocytes provided the foundation for future investigations toward translation into human in vivo studies.

## Methods

**Animals.** WT C57BL/6J mice were purchased from the Jackson Laboratory at the age of 7 weeks and allowed to acclimate in the Case Western Reserve University for 2 weeks prior to the experiments described below. Sprague-Dawley rat pups were purchased from the Charles River Laboratories at 2 days of age and sacrificed for NRVMs isolation upon arrival.

**Preparation and administration of SR9009 and GSK4112.** SR9009 was synthesized and purified in the laboratory of Thomas Burris (Department of Pharmacology and Physiology, St. Louis University, St. Louis, Missouri, USA) as previously published (13). For in vitro experiments, SR9009 was dissolved in DMSO and administered at 5 M; GSK4112 (EMD Millipore) was dissolved in DMSO and administered at 10 M using an equal volume of DMSO as control. For in vivo experiments, SR9009 was dissolved in 5% DMSO/10% Cremaphor EL (Sigma-Aldrich, C5135)/85% PBS in a working solution at 10 mg/ml. Mice were injected at a dose of 100 mg/kg/day given i.p. once daily at *zeitgeber* time 8 (ZT8). The diluent without SR9009 of the same volume was used as control.

**TAC.** All mice were C57BL/6J littermate males aged 9 weeks at the start of the experiment. Mice were anesthetized with ketamine/xylazine, mechanically ventilated (Harvard apparatus), and subjected to thoracotomy. The aortic arch was constricted between the left and right carotid arteries using a 7.0 silk suture and a 27- or 28-gauge needle as previously described (20). Chemicals were obtained from Sigma-Aldrich.

**Echocardiography.** For transthoracic echocardiography, mice were anesthetized with 1% inhalational isoflurane and imaged using the Vevo 770 High Resolution Imaging System (Visual Sonics Inc.) and the RMV-707B 30 MHz probe. Measurements were obtained from M-mode sampling, and integrated EKV images were taken in the LV short axis at the mid-papillary level.

**Blood pressure.** Conscious tail-vein systolic blood pressure was measured using the BP2000 Blood Pressure Analysis System (Visitech Systems Inc.) as recommended by the manufacturer. To allow mice to adapt to the apparatus, we performed daily blood pressure measurements for 1 week prior to beginning experiments.

**NRVMs and CF culture.** NRVMs and CFs were isolated from the hearts of 2-day-old Sprague-Dawley rat pups (Charles River Laboratories). The cells were differentially preplated for 1.5 hr. The nonattached cells were collected as NRVM and replated with 48 hr exposure to BrdU to suppress nonmyocytes. The attached cells were passaged 2–3 times to obtain CFs. NRVMs were initially plated in growth medium (DMEM supplemented with 10% FBS, 100 U/ml penicillin-streptomycin, and 2 mM L-glutamine) for 48 hr and maintained in serum-free media thereafter (DMEM supplemented with 1% insulin-transferrin-selenium liquid media supplement [Sigma-Aldrich, I3146], 100 U/ml penicillin-streptomycin). For hypertrophic stimulation, NRVM were incubated with SR9009 or GSK4112 versus DMSO for 24 hr, followed by stimulation with PE (100 $\mu$ M) for the indicated time. CFs were cultured in DMEM supplemented with 10% FBS, 100 U/ml penicillin-streptomycin, and 2 mM L-glutamine and stimulated with TGF $\beta$ 1 (eBioscience).

**Human cardiomyocytes culture.** We purchased human induced pluripotent stem cell-differentiated cardiomyocytes from Cellular Dynamics (iCell). We followed manufacturer's protocol and measured NPPB expression 24 hr after ET-1 (10 nM, Sigma-Aldrich) induction.

**Cell area measurements.** NRVM were plated on glass coverslips in 6-well dishes at a density of  $1 \times 10^5$  cells/ml. After treatments, cells were fixed in ice cold methanol, permeabilized with PBST/0.3% Triton X-100, and blocked in PBST/5% horse serum. Primary antibody was anti- $\alpha$ -actinin (Sigma-Aldrich, A7811) at 1:500. Secondary antibody (anti-mouse Alexa 488, Life Technologies) was used at 1:1,000 dilution. Coverslips were mounted on glass slides with mounting media containing DAPI. Quantitation of cardiomyocyte cell surface area was performed on anti-actinin-stained cardiomyocytes using fluorescent microscopy and ImagePro software. Analysis consisted of at least 200 cardiomyocytes in 20–30 fields at 400 $\times$  magnification. Three independent experiments were performed.

**Histological analysis.** Short-axis heart sections from the midventricle were fixed in PBS/4% paraformaldehyde and embedded in paraffin. Fibrosis was visualized using Gomori's Trichrome staining kit (Sigma-Aldrich) with quantification of fibrotic area using ImagePro software. TUNEL staining was

performed using the CardioTACS In Situ Apoptosis Detection kit (R&D Systems) according to manufacturer's instructions. Cryopreserved sections were used for myocardial capillary staining, which was performed in frozen LV sections using anti-PECAM-1 antibodies (1:200, BD Pharmingen, MEC13.3). The cardiomyocyte cross-sectional area was determined by staining with WGA Alexa 594 (Life Technologies) and analyzed using ImagePro software.

**RNA purification and quantitative PCR.** For tissue RNA, a 10–20 mg piece of mouse heart at apex was preserved in RNA Later stabilization reagent (Qiagen) followed by mechanical disruption/homogenization in Trizol (Life Technologies) on a TissueLyser (Qiagen) using stainless steel beads (Qiagen). RNA was purified from the aqueous phase using the miRNAeasy kit (Qiagen) following manufacturer's instructions. For cellular samples, total RNA from NRVM was isolated using the High Pure RNA isolation kit (Roche Diagnostics) with on-column DNAase treatment according to manufacturer's directions. Purified RNA was reverse transcribed to complementary DNA using the iScript™ RT Supermix (Bio-Rad) following manufacturer's protocol. qPCR was performed using TaqMan chemistry (Taqman Fast Advanced Master Mix, Applied Biosystems) and labeled probes from the Roche Universal Probe Library System on Applied Biosystems ViiA 7. Relative expression was calculated using the  $\Delta\Delta C_t$ -method with normalization to *Ppib* (Cyclophilin-B). Specific primer/probe sequences are available upon request. For RNA-Seq, libraries were prepared using the Illumina TruSeq Stranded Total RNA Sample Preparation kit according to the manufacturer's protocol. Singled-end sequencing (50 bp) was performed on pooled libraries in groups of 3 using an Illumina HiSeq 2500.

**RNA-Seq and ChIP-Seq analyses.** Sequencing reads generated from the Illumina platform were assessed for quality using FastQC. The reads were then trimmed for adapter sequences using TrimGalore. For RNA-Seq, reads that passed quality control were then aligned to rn6 using TopHat (21). The TopHat results were then analyzed for differential expression using Cufflinks to generate the fragments per kilobase of exon per million fragments mapped (FPKM) for each gene (22). Differential genes were identified using a significance cutoff of  $q < 0.005$  and fold change  $> 1.5$ . These genes were then subjected to further analysis. All original RNA-Seq data were deposited in the NCBI's GEO (GSE98575). For ChIP-Seq, the reads that passed quality control were aligned to mouse genome release mm9 using Burrows-Wheeler Alignment (BWA) (23). Peaks were called using MACS 1.4.2 (24). The default  $P$  value for peak detection was used ( $1 \times 10^{-5}$ ). Further annotation and analysis of the called peaks were performed using HOMER, using default settings (25). For each immunoprecipitated sample, a matching chromatin input sample was used.

**Hierarchical clustering.** The hierarchical relationship for the samples was determined using differentially expressed genes between all pairwise comparison groups. The samples were clustered using Hierarchical-Clustering v6 (Broad Institute) by pairwise average-linkage according to the distance measure using the Pearson correlation coefficient. Heatmaps and dendrograms were generated from the output of the HierarchicalClustering using Java TreeView (26).

**GSEA.** Enriched pathways were determined using GSEA v17.6 using GenePattern and the Molecular Signature Database (MSigDB; Broad Institute). The FPKM values from significantly differentially expressed genes ( $q < 0.005$  and fold change  $> 1.5$ ) as determined from the Cufflinks software were normalized for each gene across all samples, and the  $Z$  score was used as input for pathway analysis. The gene set used for comparison was the KEGG database, and enrichment significance was determined using 1000 genomes project. Pathways were considered enriched using a significance cutoff FWER  $< 0.25$ .

**Gene ontology analysis.** KEGG analysis were performed using DAVID bioinformatics suite (27).

**Mitochondrial respiration studies.** The assay was performed using Seahorse (Agilent) and following the manufacturer's published protocol. Isolated mitochondria (0.5  $\mu$ g; measured by BCA assay) were loaded per assay.

**Mitochondrial genome quantification.** Total DNA was extracted from the hearts or NRVMs using the QIAamp DNA Mini Kit (Qiagen, 51304). Mitochondrial DNA content was assessed by qPCR using primers specific for multiple mitochondrial-encoded genes (*mt-Cox1*, *mt-Nd2*, *mt-Nd1*, and *mt-Nd5*) and normalized to nuclear DNA content (a specific locus on mouse chromosome 6) using the  $\Delta\Delta C_t$  method.

**Transmission electron microscopy.** Small pieces of tissue from the LV free wall were fixed by sequential immersion in triple aldehyde-DMSO, ferrocyanide-reduced osmium tetroxide, and acidified uranyl acetate; dehydrated in ascending concentrations of ethanol; passed through propylene oxide; and embedded in Poly/Bed resin (Polysciences Inc., 21844-1). Thin sections were sequentially stained with acidified uranyl acetate, followed by a modification of Sato's triple lead stain, and examined with a JEOL 1200EX electron microscope.

**Statistics.** All statistical analyses were performed with 2-tailed Student *t* test. The significance is as labeled in figure legends and corrected for multiple comparison using Holm-Sidak method, with  $\alpha = 0.05$ .

**Study approval.** Protocols were reviewed and approved by the Case Western Reserve University Animal Care and Use Committee.

## Author Contributions

LZ and MKJ conceived and designed the research study. LZ, RZ, CLT, KS, ACG, YS, and XL conducted the experiments. LZ, RC, CF, and ACG analyzed the data. TPB provided key reagents. LZ and MKJ wrote the manuscript with input from others.

## Acknowledgments

The work is supported by NIH grant R01HL119195 (MKJ) and K01HL123551 (LZ).

Address correspondence to: Lilei Zhang, One Baylor Plaza, Room 441E, Houston, Texas 77030, USA. Phone: 713.798.2285; Email: Lilei.Zhang@bcm.edu. Or to: Mukesh K. Jain, 2103 Cornell Road, Room 4537, Cleveland, Ohio 44106-7290, USA. Phone: 216.368.3607; Email: Mukesh.jain2@case.edu.

1. Benjamin EJ, et al. Heart Disease and Stroke Statistics-2017 Update: A Report From the American Heart Association. *Circulation*. 2017;135(10):e146–e603.
2. Writing Group Members, et al. Heart Disease and Stroke Statistics-2016 Update: A Report From the American Heart Association. *Circulation*. 2016;133(4):e38–360.
3. Rajabi M, Kassiotis C, Razeghi P, Taegtmeier H. Return to the fetal gene program protects the stressed heart: a strong hypothesis. *Heart Fail Rev*. 2007;12(3-4):331–343.
4. Everett LJ, Lazar MA. Nuclear receptor Rev-erba: up, down, and all around. *Trends Endocrinol Metab*. 2014;25(11):586–592.
5. Zhu B, et al. Coactivator-Dependent Oscillation of Chromatin Accessibility Dictates Circadian Gene Amplitude via REV-ERB Loading. *Mol Cell*. 2015;60(5):769–783.
6. Zhang Y, et al. GENE REGULATION. Discrete functions of nuclear receptor Rev-erba couple metabolism to the clock. *Science*. 2015;348(6242):1488–1492.
7. Alibhai FJ, et al. Disrupting the key circadian regulator CLOCK leads to age-dependent cardiovascular disease. *J Mol Cell Cardiol*. 2017;105:24–37.
8. Zhang L, et al. KLF15 Establishes the Landscape of Diurnal Expression in the Heart. *Cell Rep*. 2015;13(11):2368–2375.
9. Lam MT, et al. Rev-Erbs repress macrophage gene expression by inhibiting enhancer-directed transcription. *Nature*. 2013;498(7455):511–515.
10. van Oort RJ, et al. MEF2 activates a genetic program promoting chamber dilation and contractile dysfunction in calcineurin-induced heart failure. *Circulation*. 2006;114(4):298–308.
11. Xu J, Gong NL, Bodi I, Aronow BJ, Backx PH, Molkentin JD. Myocyte enhancer factors 2A and 2C induce dilated cardiomyopathy in transgenic mice. *J Biol Chem*. 2006;281(14):9152–9162.
12. Papait R, et al. Genome-wide analysis of histone marks identifying an epigenetic signature of promoters and enhancers underlying cardiac hypertrophy. *Proc Natl Acad Sci USA*. 2013;110(50):20164–20169.
13. Solt LA, et al. Regulation of circadian behaviour and metabolism by synthetic REV-ERB agonists. *Nature*. 2012;485(7396):62–68.
14. Yeaman SJ, et al. Sites of phosphorylation on pyruvate dehydrogenase from bovine kidney and heart. *Biochemistry*. 1978;17(12):2364–2370.
15. Woldt E, et al. Rev-erb- $\alpha$  modulates skeletal muscle oxidative capacity by regulating mitochondrial biogenesis and autophagy. *Nat Med*. 2013;19(8):1039–1046.
16. Hannenhalli S, et al. Transcriptional genomics associates FOX transcription factors with human heart failure. *Circulation*. 2006;114(12):1269–1276.
17. Kojetin DJ, Burriss TP. REV-ERB and ROR nuclear receptors as drug targets. *Nat Rev Drug Discov*. 2014;13(3):197–216.
18. Banerjee S, et al. Pharmacological targeting of the mammalian clock regulates sleep architecture and emotional behaviour. *Nat Commun*. 2014;5:5759.
19. Harding HP, Lazar MA. The orphan receptor Rev-Erba alpha activates transcription via a novel response element. *Mol Cell Biol*. 1993;13(5):3113–3121.
20. Hu P, Zhang D, Swenson L, Chakrabarti G, Abel ED, Litwin SE. Minimally invasive aortic banding in mice: effects of altered cardiomyocyte insulin signaling during pressure overload. *Am J Physiol Heart Circ Physiol*. 2003;285(3):H1261–H1269.
21. Trapnell C, Pachter L, Salzberg SL. TopHat: discovering splice junctions with RNA-Seq. *Bioinformatics*. 2009;25(9):1105–1111.
22. Trapnell C, et al. Transcript assembly and quantification by RNA-Seq reveals unannotated transcripts and isoform switching during cell differentiation. *Nat Biotechnol*. 2010;28(5):511–515.
23. Li H, Durbin R. Fast and accurate short read alignment with Burrows-Wheeler transform. *Bioinformatics*. 2009;25(14):1754–1760.
24. Zhang Y, et al. Model-based analysis of ChIP-Seq (MACS). *Genome Biol*. 2008;9(9):R137.
25. Heinz S, et al. Simple combinations of lineage-determining transcription factors prime cis-regulatory elements required for macrophage and B cell identities. *Mol Cell*. 2010;38(4):576–589.
26. Saldanha AJ. Java Treeview—extensible visualization of microarray data. *Bioinformatics*. 2004;20(17):3246–3248.
27. Huang da W, Sherman BT, Lempicki RA. Bioinformatics enrichment tools: paths toward the comprehensive functional analysis



- of large gene lists. *Nucleic Acids Res.* 2009;37(1):1–13.
28. Shen Y, et al. A map of the cis-regulatory sequences in the mouse genome. *Nature.* 2012;488(7409):116–120.
29. He A, Kong SW, Ma Q, Pu WT. Co-occupancy by multiple cardiac transcription factors identifies transcriptional enhancers active in heart. *Proc Natl Acad Sci USA.* 2011;108(14):5632–5637.